Article

The combined influences of hot streak and swirl on the cooling performances of C3X guide vane with or without TBCs

Li Shi[1,*], Hanze Huang[1], Yuanfeng Lu[1], Shunsheng Xu[1] and Chen Ge[2]

[1] School of Mechanical Engineering, Xiangtan University, Xiangtan 411105, China; xtuhhz@163.com (H.H.); xtulyf@126.com (Y.L.); xtuxss@163.com (S.X.)

[2] School of Energy and Environmental Engineering, University of Science and Technology Beijing, Beijing 100083, China; ustbgec@163.com (C.G.)

* Correspondence: shili@xtu.edu.cn ; Tel.: +86-731-5829-2209

Received: date; Accepted: date; Published: date

Abstract: This paper studied the combined influences of the hot streak and swirl on the cooling performances of the NASA C3X guide vane coated with or without TBCs. The results show that: (1) Even under uniform velocity inlet conditions, the hot streak core can be stretched as it impinges the leading edge which causes higher heat load on the suction side of the forward portion. (2) The swirl significantly affects circumferential and radial migration of the hot streak core in the NGV passage. On the passage inlet plane, positive swirl leads to a hotter tip region on the suction side. In comparison, negative swirl leads to a hotter hub region on the pressure side. (3) Under the influence of swirl, migration of coolant improve the coverage of film cooling close to the midspan, while in the regions close to the hub and tip end-wall, the overall cooling performance decrease simultaneously. (4) In the regions with enough internal cooling, the cooling effectiveness increment is always larger than that in other regions. Besides, the overall cooling effectiveness increment decreases on the region covered by film cooling for the coated vane, especially in the region with negative local heat flux.

Keywords: hot streak; swirl; turbine vane; thermal barrier coatings; overall cooling effectiveness

1. Introduction

Gas turbine, as one of the most advanced thermal prime mover, has achieved rapid development in aviation, power generation, shipping, petrochemical and other industries [1]. Because of the continuing demand for improvement of thermal efficiency and power, typical turbine inlet temperature has exceeded the highest allowable material temperature of airfoil [2]. Under such harsh running conditions, the turbine vane has to be protected to guarantee safe running conditions [1-2]. Typical advanced cooling techniques include internal cooling, film cooling as well as thermal barrier coatings (TBCs) [3]. In the internal cooling technique, coolant from the last stage of the compressor enters the airfoil from the root, through internal cooling channels and exhaust from the tip to cool down the airfoil [1]. In the film cooling technique, coolant from separate rows of film cooling holes forms a protective layer of film cooling to defense the vane against the onslaught of mainstream [2]. Because of the limited gains of further improvement of the film cooling performance, typically advanced gas turbine airfoil usually incorporates TBCs and film cooling techniques [3-4].

Some researchers have studied the overall cooling performances of a coated vane or blade with uniform temperature inlet conditions [5-7]. Liu et al. [5] found the influence of inlet temperature of mainstream on temperature variation of coatings surface was larger than that of the heat transfer coefficient of cooling channels. Prasert P et al. [6] claimed that increment of turbulence intensity had a smaller influence on decreasing the average temperature. Shi et al. [7] found that TBCs showed both the positive and negative roles in improving cooling performance for the coated vane with or

 doi:10.20944/preprints202104.0568.v1

without film cooling. However, in real turbine stage inlet boundary, the distributions of velocity, turbulence and temperature show large non-uniform both in radial and circumferential directions [8]. The non-uniform distributions of velocity and turbulence can be caused by intensive residual swirl flow at the exit of lean-burn combustor which is widely applied to ensure combustion stability and lower NO_x emissions [9]. The non-uniform distributions of temperature named as hot streak (HS) is caused by the discrete nature of fuel nozzles and coolant flow of combustor lining [8]. It is noted that a 25 K under prediction of the blade metal temperature can cause a halving of blade life span [9]. However, for typical military engines, the temperature ratio can reach up to 1.24 of the mass averaged temperature [10]. Thus, it is important to examine the influence of the non-uniform inlet boundary condition to maximize turbine performance and reliability.

Some researchers have researched the individual influence of swirl and hot streak on the heat transfer characteristic and film cooling performance of the uncoated vane or blade. Povey et al. [11-12] and Stewart et al. [13] have made good efforts to measure the radial temperature profile at the exit of the lean-burn combustor. The measured temperatures ratio was range from 0.59 to 1.24, for different mean temperatures. However, measurements of whole field temperature measurements are still limited in the open literature. Simone et al. [14] found hot streak aligned with the leading edge lead to higher thermal load on the suction side of the vane because of the mixing effect of the vane wake. The intensive residual swirl flow at the exit of the lean-burn combustor influences the passage secondary flow, and thus the aerodynamic and heat transfer performance. Feng et al. [15] claimed that the hot streak aligned with the passage lead to less heat load on the vane surface than that aligned with the leading edge. Intensive residual swirl flow at the exit of the lean-burn combustor changed the incidence of vanes and thus twisted the stagnation line. Qureshi et al. [16] found that swirl flow changed the vortex pattern and thus the pressure loads distribution of the first stage vane passage. Jacobi et al. [17-18] found the swirl flow-induced vortices at the leading edge of the vane. Qureshi et al. [19-20] found the swirl flow changed the strength of the passage vortex and increase the Nusselt number on both hub and tip of the airfoil. Werschnik et al. [21] claimed that higher turbulence intensity induced by swirl flow increased the heat transfer and thus decreased the film cooling effectiveness near the hub region. Schmid et al. [22] found that the negative swirl flow declined the aerodynamic penalty in the turbine.

Even though there is much literatures study the individual influence of swirl and hot streak, few studies consider the combined effects on the temperature distribution and heat loads over the vane surface. Also, there are no results in the open literatures about the combined influences of swirl and hot streak on the cooling performances of a coated vane or blade. Based on these viewpoints, conjugate heat transfer (CHT) analyses have been applied to the NASA C3X guide vane with or without TBCs. Firstly, baseline cases with or without TBCs under the uniform turbine inlet boundary conditions have been examined. Then, six other cases under the individual effects of swirl and hot streak or their combined effect have been studied. The objective of this study is to reveal the TBCs insulation characteristics and cooling performances under the combined effects of hot streak and swirl to provide guide line for cooling arrangements design process of the coated vane.

2. Numerical methods

2.1. Geometry structure and mesh generation

The film-cooled NASA guide C3X vane used in this study is a 2D stainless steel nozzle guide vane (NGV) reported by Hylton et al. [23-24]. The span and axial chord are 77.22 mm and 78.16 mm [23-24]. Three irregular-shaped coolant channels span the forward portion of the vane which feed rows of film cooling holes with the same diameter of 0.1 cm, see in Figure 1(a). In addition, 48 cylindrical film cooling holes are mounted on the leading edge with the spanwise angle of 45°. Furthermore, 52 cylindrical film cooling holes which orthogonal to the span are mounted on both sides of the vane, see in Figure 1(a). Besides, ten radial cooling channels locate along the axial of the aft portion of the vane. The forward portion and aft portion of the vane is split by a thermal barrier

Preprints (www.preprints.org) | NOT PEER-REVIEWED | Posted: 21 April 2021 doi:10.20944/preprints202104.0568.v1

[23]. A hybrid grid approach is adapted with commercial software ANSYS ICEM CFD 18.2. The aft portion of the vane is meshed with unstructured hexahedral mesh, while the forward portion is meshed with tetrahedral grids. An O-grid scheme with 20 layers of hexahedral elements is applied to the boundary layer along the entire surface of the vane, see in Figure 1(b). Three mesh models with 10.1 million, 15.4 million and 20.9 million grid elements are used to assure grid independence. A grid independence study is initially undertaken for the uniform inlet case which is based on the experiment Case 44344 reported by Hylton et al. [23-24]. In this case, the total temperature, pressure and turbulence intensity are 701 K, 285.13 kPa and 6.5 %, respectively [23]. The mass flow rates of coolant are 0.638×10^{-2} kg/s, 0.752×10^{-2} kg/s and 0.134×10^{-1} kg/s for the inlet of leading edge (LE), pressure side (PS) and suction side (SS) coolant channels, respectively [24]. Inlet total temperature of LE, PS and SS coolant channels are 602.86 K, 581.83 K and 595.85 K, with the same turbulence intensity of 5 % [23-24]. The inlet and outlet conditions of ten radial cooling channels are consistent with the conditions provided in Ke Z et al. [25]. Figure 2 presents the normalized total pressure and static temperature along the midspan among three meshes and experiment results of the Case 44344 [23-24]. The references total pressure and static temperatures are 285.13 kPa and 701 K, respectively. For the normalized total pressure, the predicted data are very close to the experimental results, except for the region between 25 % C_{ax} and 50 % C_{ax}. For the normalized total temperature, calculated values are also in close agreement with the experimental results. Overall, the maximum deviations between experimental data and calculated values of different meshes are smaller than 5 %. The medium-mesh with 15.4 million grid elements is selected for hot streak and swirl simulation, see in Figure 1(b).

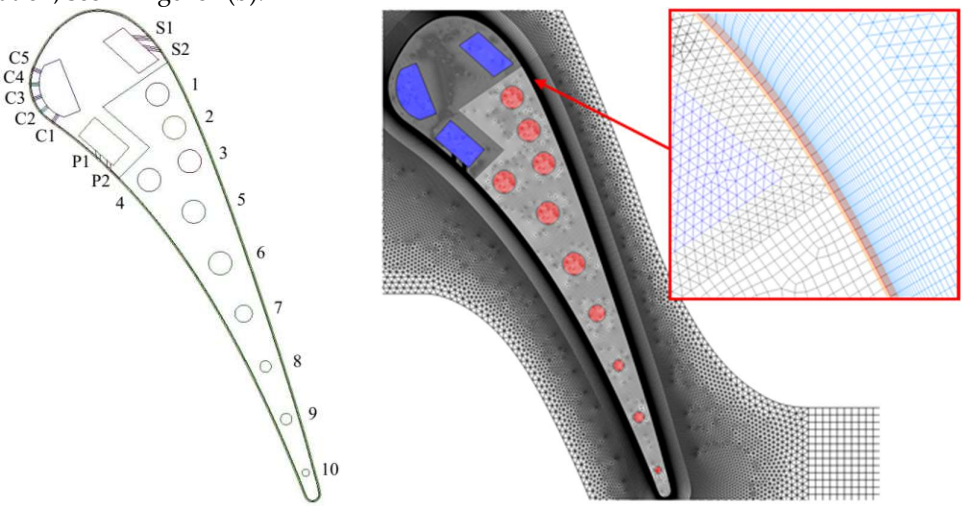

(**a**) Vane (**b**) Mesh

Figure 1. Vane structure and mesh.

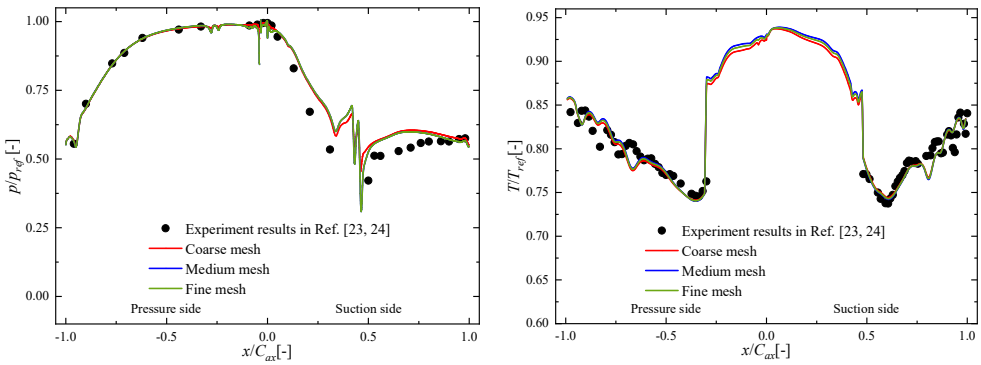

(**a**) Pressure profile (**b**) Temperature profile

Figure 2. Grid independence test.

Preprints (www.preprints.org) | NOT PEER-REVIEWED | Posted: 21 April 2021 doi:10.20944/preprints202104.0568.v1

Table 1. Boundary conditions.

Gas	Boundary	Value
Mainstream	Total temperature (K)	701
	Total pressure (kPa)	285.13
	Outlet pressure (kPa)	170.42
	Turbulence intensity (%)	6.5
Coolant	Mass flow of LE coolant (kg/s)	0.638×10-2
	Temperature of LE coolant (K)	602.86
	Mass flow of PS coolant (kg/s)	0.752×10-2
	Temperature of PS coolant (K)	581.83
	Mass flow of SS coolant (kg/s)	0.134×10-1
	Temperature of SS coolant (K)	595.85
	Turbulence intensity (%)	5

2.2. Thermal parameter definition

For a typical time-mean temperature field in turbine inlet, the region with peak temperature locates near the midspan, while near the tip and hub of the vane, there are cool regions with lower temperatures. Temperature distortion factors (TDFs) are used to quantify temperature non-uniformity of hot streak [9]. There are several definitions of TDFs in current studies [9-11]. The overall TDF (OTDF) is a measure of the divergence of the hottest gas streak from the mean temperature [9]. The radial TDF（RTDF）is a measure of the non-uniformity of the circumferentially averaged temperature field [10]. Local OTDF (LOTDF) and local RTDF (LRTDF) are used to describe the form of the temperature profile. The definitions are shown as follows:

$$\mathrm{OTDF}=\frac{T_{4,\max}-\overline{T}_4^{\mathrm{area}}}{\Delta T_{\mathrm{comb}}} \tag{1}$$

$$\mathrm{RTDF}=\frac{\overline{T}_{4,\max}^{\mathrm{circ}}-\overline{T}_4^{\mathrm{area}}}{\Delta T_{\mathrm{comb}}} \tag{2}$$

$$\mathrm{LOTDF}=\frac{T_4-\overline{T}_4^{\mathrm{area}}}{\Delta T_{\mathrm{comb}}} \tag{3}$$

$$\mathrm{LRTDF}=\frac{\overline{T}_4^{\mathrm{circ}}-\overline{T}_4^{\mathrm{area}}}{\Delta T_{\mathrm{comb}}} \tag{4}$$

$$\Delta T_{\mathrm{comb}}=\overline{T}_4^{\mathrm{area}}-\overline{T}_3^{\mathrm{area}} \tag{5}$$

Where $\overline{T}^{\mathrm{area}}$ is the area mean temperature, $\overline{T}^{\mathrm{circ}}$ is the circumferential mean temperature which is a function of radial height, ΔT_{comb} is the temperature rise across the combustor, T is the local temperature. The subscript "max" identifies the maximum [11]. Besides, the subscripts "3" and "4" identifies that the temperature has been taken at the combustor inlet and exit planes, respectively [12]. Swirl number (SN) is a measure of the swirl intensity [11-12]. In addition, swirl angle α and pitch angle β are also used in some studies. The definitions are shown as follows:

$$SN=\frac{\int_0^{r_0}(\rho u_{\mathrm{ax}}u_{\tan})r^2dr}{\int_0^{r_0}(\rho u_{\mathrm{ax}}^2)rdr} \tag{6}$$

$$\alpha=\arctan(\frac{u_{\tan}}{u_{\mathrm{ax}}}) \tag{7}$$

$$\beta=\arctan(\frac{u_{\mathrm{rad}}}{u_{\mathrm{ax}}}) \tag{8}$$

Preprints (www.preprints.org) | NOT PEER-REVIEWED | Posted: 21 April 2021 doi:10.20944/preprints202104.0568.v1

Where ρ is the density of mainstream, u_{ax}, u_{rad} and u_{tan} is the inlet axial, radial and tangential velocity component of the mainstream, see in Figure 3 [8, 9].

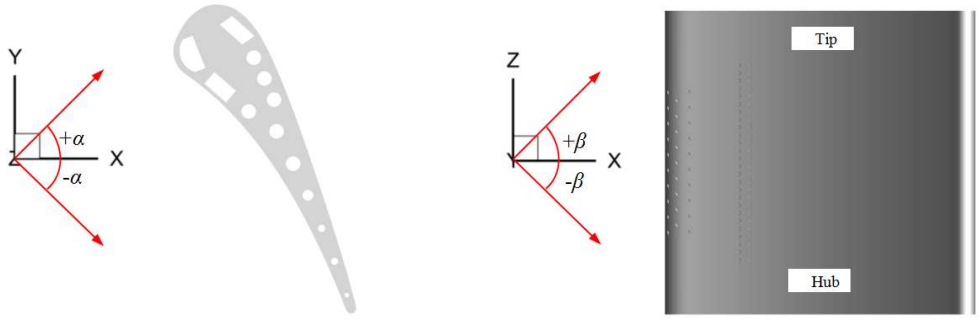

(**a**) Swirl angle α (**b**) Pitch angle β

Figure 3. Definitions of swirl angle and pitch angle.

The overall cooling effectiveness is used to quantify cooling performances of airfoil. Increment of overall cooling effectiveness ($\Delta\varphi$) is used to quantify the cooling performance increment because of the coatings for the coated vane [11]. The definitions are as follows:

$$\varphi = \frac{T_\infty - T}{T_\infty - T_c} \tag{9}$$

$$\varphi_{TBC} = \frac{T_\infty - T_{\mathrm{TBC}}}{T_\infty - T_c} \tag{10}$$

$$\Delta\varphi = \varphi_{\mathrm{TBC}} - \varphi \tag{11}$$

where T is the local vane surface temperature of the uncoated vane, T_c is the inlet temperature of coolant, T_{TBC} is the local subtract surface temperature of the coated vane, T_∞ is the inlet temperature of the mainstream, T' is the coatings surface temperature, see in Figure 4 [11].

Table 2. Material properties.

Material	Temperature (K)	Density (kg/m3)	Specific heat (J/kg·K)	Thermal conductivity (W/m·K)
Gas		Ideal gas	C_p=938+0.196T	k_f=0.0102+5.8×10-5T
TC		5650	483	1.05
TGO	298-1273	3978	857	25.2
BC		7320	501-764	4.3-16.1
Subtract		8030	502	$k(T)$=0.0115T+9.9105

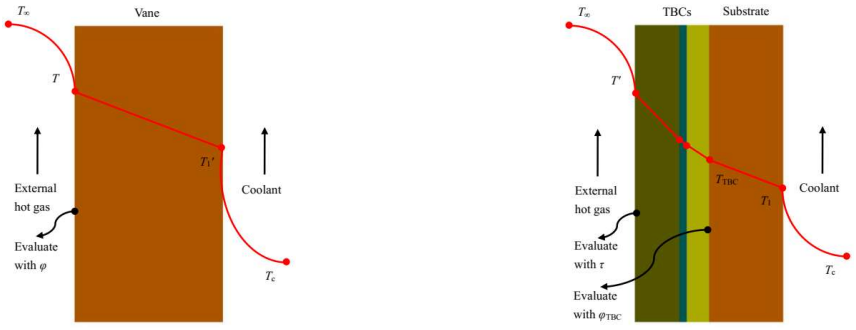

(**a**) Uncoated vane (**b**) Coated vane

Figure 4. Thermal parameters definition for uncoated vane and coated vane.

Preprints (www.preprints.org) | NOT PEER-REVIEWED | Posted: 21 April 2021 doi:10.20944/preprints202104.0568.v1

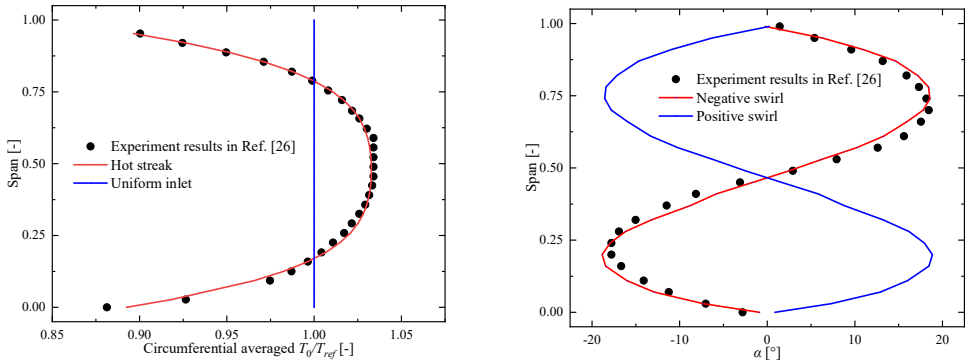

(**a**) Temperature profile (**b**) Swirl angle profile

Figure 5. Circumferential averaged temperature and swirl angle profiles.

Table 3. Definition of the simulation cases.

Case No.	Definition of cases.	Vane type	Temperature istribution	Swirl orientation
1	Uniform inlet condition for the uncoated vane	Uncoated vane	Uniform	No swirl
2	HS only inlet condition for the uncoated vane	Uncoated vane	Hotstreak	No swirl
3	HS and positive swirl inlet condition for the uncoated vane	Uncoated vane	Hotstreak	Positive swirl
4	HS and negative swirl inlet condition for the uncoated vane	Uncoated vane	Hotstreak	Negative swirl
5	Uniform inlet condition for the coated vane	Coated vane	Uniform	No swirl
6	HS only inlet condition for the coated vane	Coated vane	Hotstreak	No swirl
7	HS and positive swirl inlet condition for the coated vane	Coated vane	Hotstreak	Positive swirl
8	HS and negative swirl inlet condition for the coated vane	Coated vane	Hotstreak	Negative swirl

2.3. Boundary conditions

In this work, eight cases with different temperature distribution and swirl orientations are molded, as shown in Table 3. Case 1 and Case 4 with uniform temperature inlet conditions are molded as the baseline cases for the uncoated vane and coated vane, respectively. The boundary conditions of mainstream and coolant ejection are based on the experiment data of the Case 44344 reported by Hylton et al. [23-24], as shown in Table 1. For the coated vane, three coating layers are added upon the external surface of the substrate. The thickness definition of the bond coating (BC), thermally grown oxide (TGO) and top coating (TC) are 150 μm, 10 μm and 300 μm which are based on the coated vane reported by Liu et al. [5]. The material properties of different layers are shown in Table 2. To study the individual influence of hot streak, temperature profiles with the mass averaged total temperature of 701 K are specified at the stage inlet of the Case 2 and Case 5 for the uncoated vane and coated vane, respectively. The temperature ratio profile which fitted by a polynomial function of order four is based on the experiment results reported by Koupper et al. [26]. In Figure 5(a), it can be observed that the ratio of the maximum of circumferential averaged temperature to the mass averaged total temperature is about 1.03, while the minimum is about 0.88, for the whole stage inlet plane. Hot streak temperature profiles with positive or negative inlet swirl are specified at the stage inlet planes of the Case 3 and Case 4 for the uncoated vane, and at the stage inlet planes of the Case 7 and Case 8 for the coated vane. Figure 6 and Figure 7 show the distribution of hot streak, swirl angle as well as velocity vectors at the stage inlet plane. The swirl angle profile is also based on the experiment results reported by Koupper et al. [26]. In the radial

Preprints (www.preprints.org) | NOT PEER-REVIEWED | Posted: 21 April 2021 doi:10.20944/preprints202104.0568.v1

direction, the maximum swirl angle is about 18.5° which locates at the 80 % span, while the minimum locates at the 20 % span, see in Figure 5(b). Both the hot streak temperature and swirl angle profile are defined with the user-defined function (UDF) method with commercial software ANSYS [27].

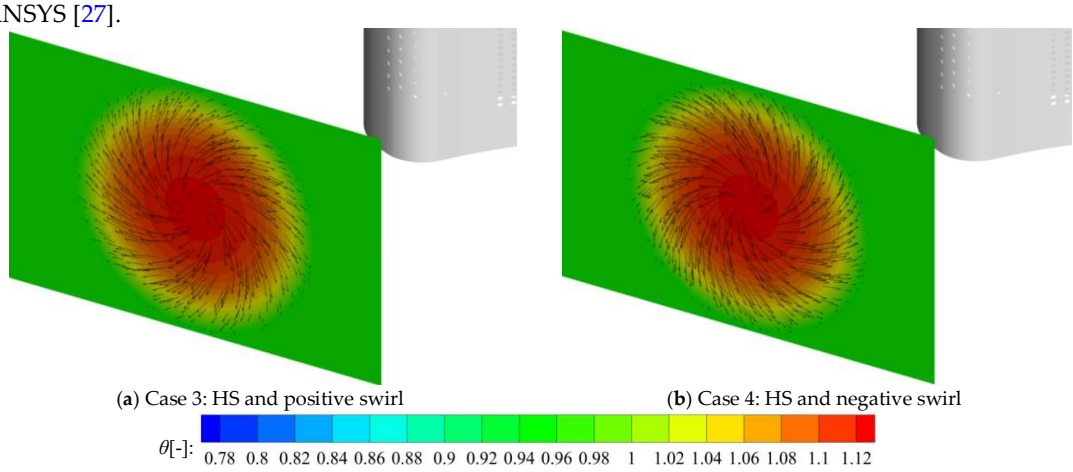

Figure 6. Hot streak and velocity vectors distribution at the stage inlet plane.

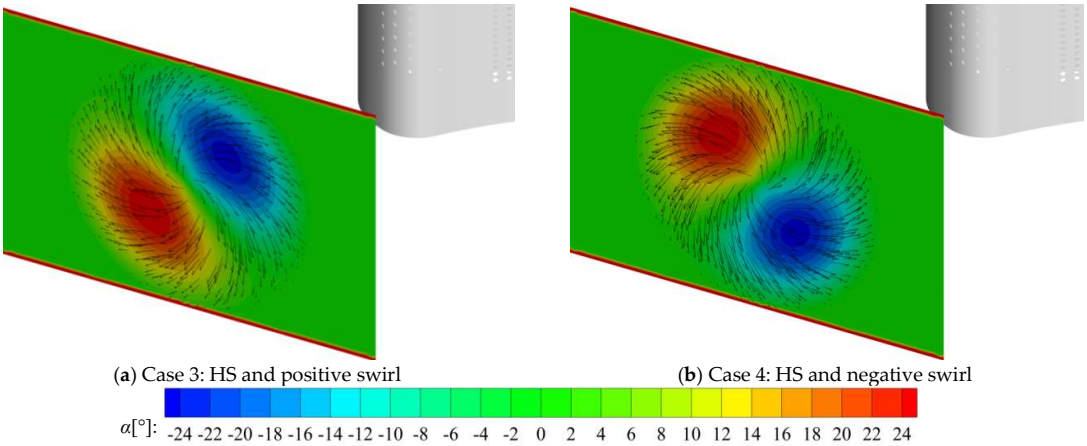

Figure 7. Swirl angle and velocity vectors distribution at the stage inlet plane.

3. Discussion

3.1. Influence of swirl on the aerodynamics characteristics

Figure 8 shows the temperature contours and hot streak core which are visualized through the iso-surface of total temperature at 701 K, for different cases. For the uniform inlet case, a local maximum of static temperature can be observed in the region close to the stagnation line, see in Figure 8(a). Further along the suction side, strong acceleration of the mainstream rapidly decreases the static temperature. In comparison, the temperature keeps at a high value until the region close to the trailing edge on the pressure side where close to the stagnation line of the neighboring vane. For the hot streak only case, most part of the vane surface on the pressure side is flooded with the hot streak core, see in Figure 8(b). In comparison, only part of the forward portion of the vane is covered with the hot streak core on the suction side. Under the influence of positive swirl, hot streak core moves slightly toward the hub region on the pressure side, see in Figure 8(c). In comparison, it moves slightly toward the tip region on the pressure side under the influence of the negative swirl, see in Figure 8(d).

Figure 9 shows the temperature and velocity vectors distribution at the cutting plane of -10 % C_{ax}, for different cases. The origin of coordinates locates in the stagnation line at the midspan. For the hot streak only case, it is clear the hot streak core is redistributed as it impinge the leading edge,

Preprints (www.preprints.org) | NOT PEER-REVIEWED | Posted: 21 April 2021 doi:10.20944/preprints202104.0568.v1

see in Figure 9(b). Higher temperature along with shorter circumferential length scales can be observed on the suction side. As expected, swirl changes the flow field, and thus stretches the hot flow both in circumferential and radial directions, see in Figure 9(c) and Figure 9(d). For the hot streak and positive swirl case, temperature increase close to the tip region on the suction side, and the hub region on the pressure side, see in Figure 9(c). In addition, a pair of counter-rotating vortices locates near the tip region. Thus, gas with a relatively smaller positive incidence locates close to the hub region. Compare with the hot streak only case, temperature increases close to the hub region on the suction side, and close to the tip region on the pressure side, see in Figure 9(d). Besides, a pair of counter-rotating vortices locates close to the hub region.

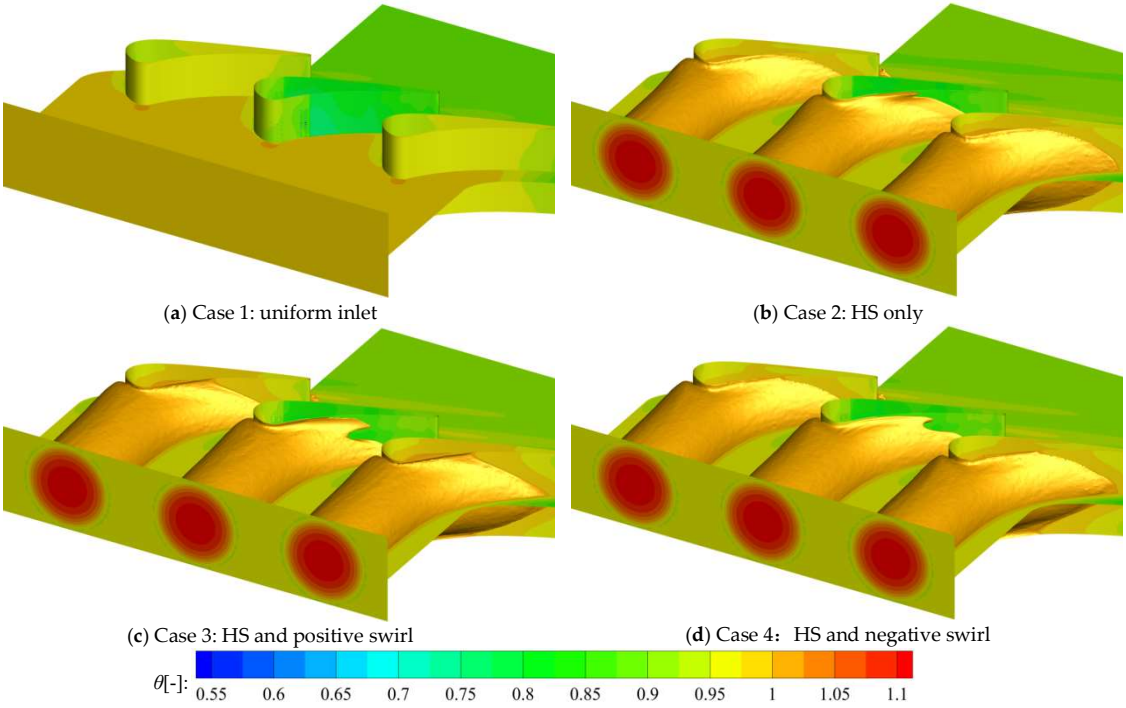

Figure 8. Stretching of hot streak core for different cases.

Figure 10 shows the temperature profiles both in circumferential and radial directions at the plane of stage inlet and -10 % C_{ax}. Compare Figure 10(a) with Figure10(c), the shape of NGV passage seems to have a relatively small influence on the local temperature distribution both in circumferential and radial directions, for the uniform inlet case. For the hot streak only case, there is also a relatively smaller difference in radial directions, see in Figure 10(a) and Figure 10(b). A local maximum temperature which is about 784 K locates close to the midspan, for the both cutting planes. In circumferential directions, much flatter temperature profile locates on the pressure side at -10 % C_{ax} plane, see in Figure 10(d). It is clear that temperature decreases from 784 K at stagnation line to 701 K at about -33 % pitch length on the pressure side, while at about 30 % pitch length on the suction side. Compare with the hot streak only case, the temperature drops are about 2.8 K, for the Case 3 and Case 4, see in Figure 10(b). In comparison, temperature increase close to the tip and hub region. Under the influence of positive swirl, there is a clear increment of temperature close to the tip region compared with other cases, see in Figure 10(b). A local maximum can be noticed close to the 55 % span which is about 781.7 K, for the hot streak and positive case. In comparison, negative swirl leads to a hotter hub region, where a local maximum located close to the 45 % span which is about 782.1 K, for hot streak and negative case, see in Figure 10(b). In circumferential directions, flatter temperature profiles locate on the pressure side at -10 % C_{ax} plane, see in Figure 10(d). Local minimum can be noticed close to about 14 % pitch length, for the Case 3 and Case 4. Considering the significant difference in temperature and velocity vector distribution, the aerodynamics and heat transfer characteristics of NGV under the combined influence of hot streak,

Preprints (www.preprints.org) | NOT PEER-REVIEWED | Posted: 21 April 2021 doi:10.20944/preprints202104.0568.v1

swirl and shape of NGV passage should be clearly revealed. Their negative influences should be lessened as much as possible.

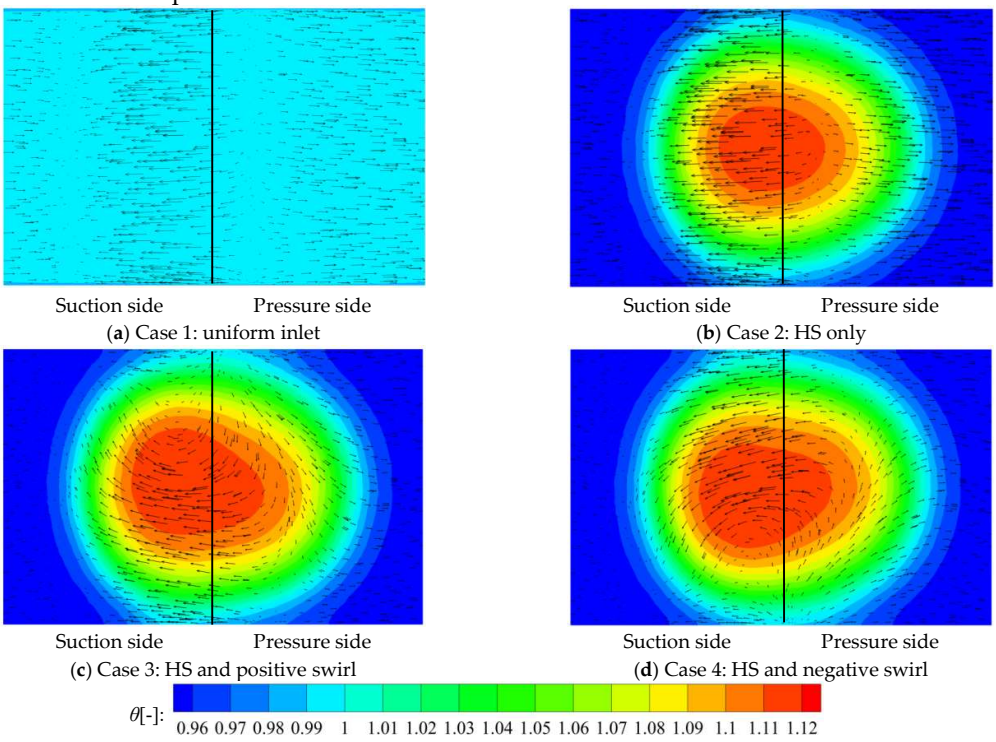

Figure 9. Temperature and velocity vector distribution at the cutting plane of -10 % C_{ax}.

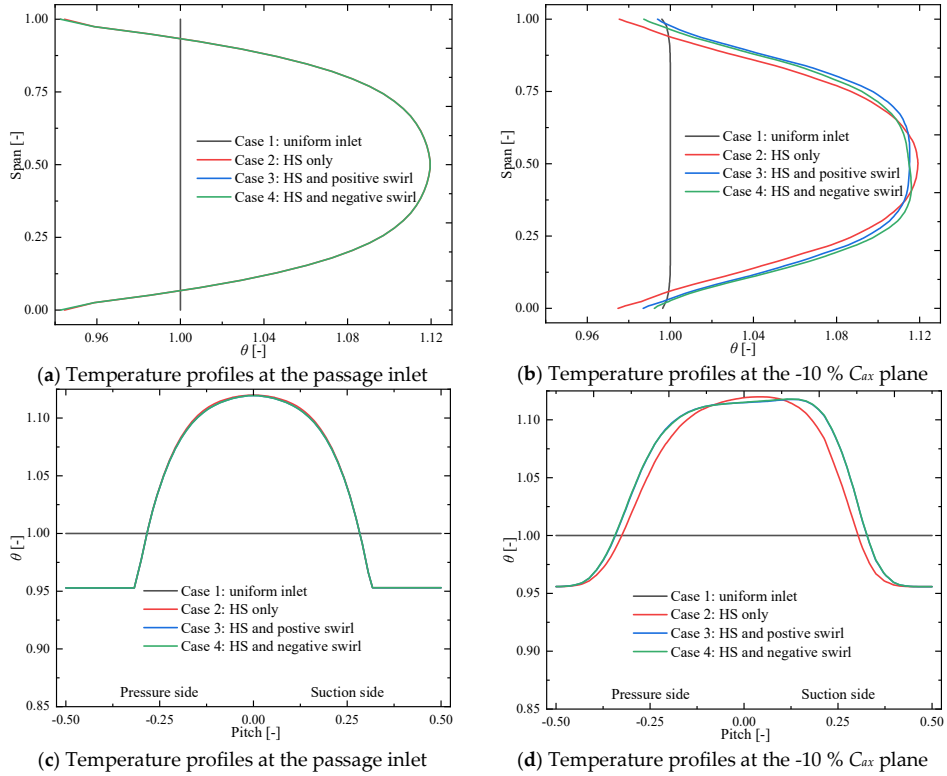

Figure 10. Local temperature profiles along the circumferential and radial directions.

3.2. Influence of hot streak and swirl on the cooling performance of the uncoated vane

Preprints (www.preprints.org) | NOT PEER-REVIEWED | Posted: 21 April 2021 doi:10.20944/preprints202104.0568.v1

Figure 11 shows the streamline pattern of coolant ejected from film cooling holes located in the leading edge, pressure side and suction side, for different cases. For the uniform inlet case, coolant exhausted from rows C1 to C3 passes downstream the pressure side, while coolant from rows C4 and C5 pass towards the suction side. As it passes through the vane surface, coolant migrates radically toward the tip region on the pressure side, see in Figure 11(a). In comparison, the radical migration of coolant is suppressed by the secondary flow channel vortex on the suction side [23-24]. On the downstream of pressure side, most of the coolant from the leading edge is pushed to lift off and reattach on the far downstream of the vane surface after it impinges the downstream cooling film. In comparison, homogeneous film coverage can be noticed on the suction side. For the hot streak only case, there is no noticeable difference in the streamline pattern of coolant, see in Figure 11(b). Under the influence of positive swirl, hot flow with negative incidence in the tip region transports the coolant toward the midspan. In the hub region, the radical migration of coolant is also enhanced by the hot flow with positive incidence, especially for the coolant from the leading edge film cooling holes, see in Figure 11(c). For the hot streak and positive case, film coolant is also transported to the midspan, see in Figure 11(d). The difference of coolant streamline pattern between two cases is that, relatively larger ejection incidence of film coolant can be observed in the tip region, for the hot streak and positive case. In comparison, larger ejection incidence of film coolant can be observed close to the hub region, for the hot streak and negative case.

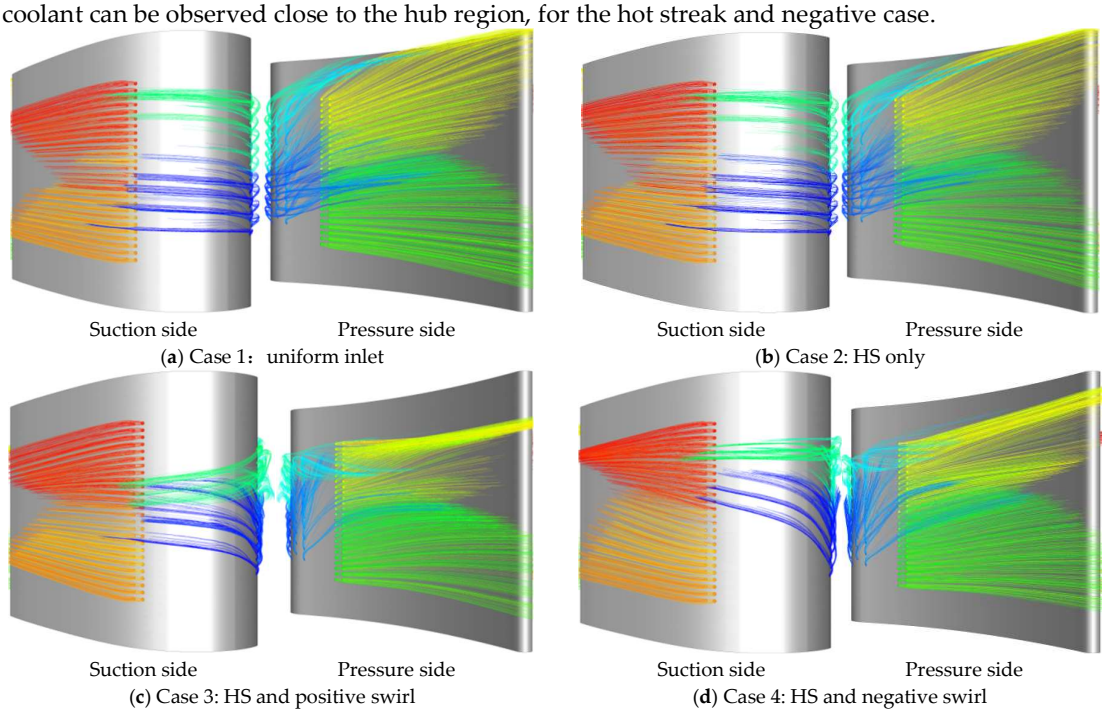

Figure 11. Streamline pattern of coolant for different cases.

Figure 12 shows the distributions of overall cooling effectiveness on the external surface of the uncoated vane, for different cases. For the uniform inlet case, the lowest overall cooling effectiveness can be observed close to the hub and tip regions where close to the stagnation line and uncovered by film cooling, see in Figure 12(a). On the pressure side, coolant exhausts from rows C1 to C3 thrust the boundary layer and reattaches on the downstream of the vane surface. Therefore, regions close to the exits of row C3 cooling holes cannot be effectively covered by film cooling, especially for the film cooling holes close to the inlet of the PS coolant channels. On the suction side, homogeneous film coverage leads to relatively more uniform total cooling effectiveness distributions. On the aft portion of the vane, a local minimum appears between two alongside radial cooling channels, and a local maximum close to a radial channel [23]. Besides, the overall cooling effectiveness of the hub is much lower than that of the tip because of the heating of coolant in the radial direction [24]. For the hot streak only case, overall cooling effectiveness decreases

Preprints (www.preprints.org) | NOT PEER-REVIEWED | Posted: 21 April 2021 doi:10.20944/preprints202104.0568.v1

significantly over the vane surface, especially on the midspan of forward portion where under the direct impingement of hot streak, see in Figure 12(b). Compare with the hot streak only case, the overall cooling effectiveness of the Case 3 and Case 4 increase in the region close to the midspan of forward portion. In comparison, it decreases in the tip and hub regions in the forward portion of the vane, see in Figure 12(c) and Figure 12(d). On the aft portion of the vane, the overall cooling effectiveness decreases because of the circumferential stretching of hot fluid for the Case 3 and Case 4.

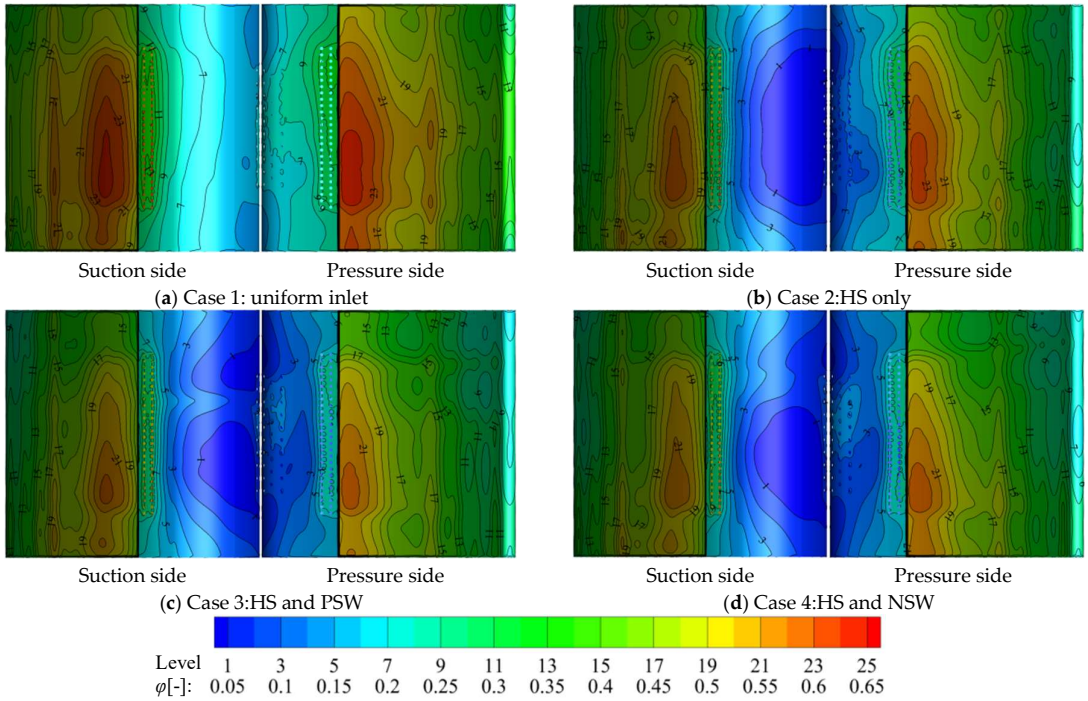

Figure 12. Overall cooling effectiveness distribution for different cases.

Figure 13 shows the dimensionless pressure and overall cooling effectiveness profiles along the vane surface at cuttings planes of the 25 % span, 50 % span and 75 % span, for different cases. It is clear that the change rules of the total pressure show the same trend, for different cases. A local maximum can be observed in the region close to the stagnation line. Further along the suction side, strong acceleration of the mainstream leads to a rapid decrease of pressure. In the region between 25 % C_{ax} and 50 % C_{ax}, coolant ejection from leading edge and suction side lead to fluctuations of pressure profile [23]. On the pressure side, the pressure keeps at a high value until the region close to the trailing edge where close to the stagnation line of the neighboring vane [24]. In Figure 13, higher fluid temperature together with less coolant lead to lower overall cooling performance on the forward portion of the vane, where the local minimum appears close to the stagnation line. As described, two irregular-shaped coolant channels along with 100 cylindrical film cooling holes are mounted on the pressure side, while only one channel with 52 holes locates close to the suction side [23-24]. Thus, rapid increment of cooling effectiveness can be observed along the pressure side, for the uniform inlet case, see in Figure 13. Although under the influence of lower fluid temperature, relatively lower cooling effectiveness can be observed on the suction side. Further downstream, the strong shock along with the transition of the boundary layer leads to a rapid decrease of cooling performance over the vane surface [23-24]. For the hot streak only case, the decrease amplitude of cooling effectiveness on the suction side is larger than that of the pressure side, see in Figure 13. Compare with the uniform inlet case, the overall cooling effectiveness reduces from about 0.294 to 0.239, a reduction of about 18.7 % at the -25 % C_{ax} of the midspan on the pressure side, for the hot streak the only case. In comparison, the overall cooling effectiveness reduces from 0.203 to 0.049, a reduction of about 76 % at the 25 % C_{ax} of the midspan on the suction side. On the aft portion of the vane, the decrease of cooling effectiveness on the trailing edge is larger than that of other regions.

Preprints (www.preprints.org) | NOT PEER-REVIEWED | Posted: 21 April 2021 doi:10.20944/preprints202104.0568.v1

Under the influence of swirl, the cooling effectiveness decrease on the most parts of the vane surface, except for the suction side of the forward portion for the hot streak and swirl cases, see in Figure 13. As mentioned above, temperature increases close to the tip region on the suction side and the hub region on the pressure side for the Case 3. Thus, the overall cooling effectiveness of the Case 3 is smaller than that of the Case 4 at the 25 % span on the pressure side and at the 75 % span on the suction side. Compare with that of the Case 4, the overall cooling effectiveness reduces from about 0.402 to 0.375, a drop of about 6.7 % at the -75 % C_{ax} of the 25 % span on the pressure side. On the suction side, the overall cooling effectiveness reduces from 0.414 to 0.388, a reduction of about 6.3 % at the 75 % C_{ax} of the 75 % span. Considering the significant decline of cooling performance on the hub and tip region for the hot streak and swirl cases, enhancing cooling arrangements design are necessary in those regions.

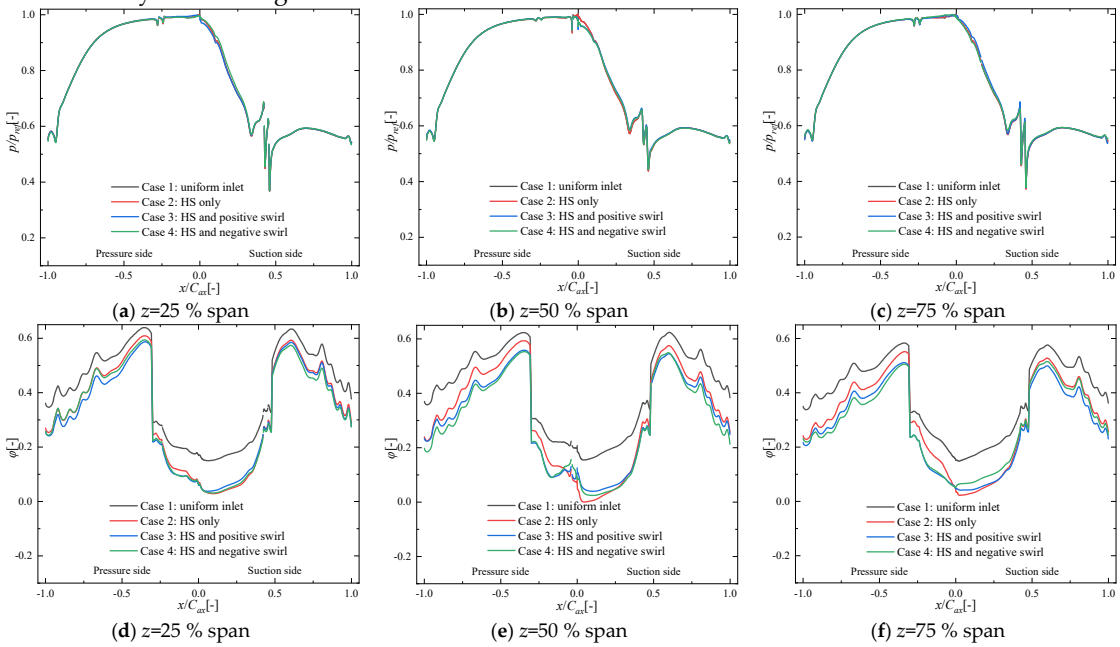

Figure13. Pressure and overall cooling effectiveness profiles along the vane surface.

3.3. Influence of hot streak and swirl on the heat transfer characteristics

Figure 14 shows the distribution of local heat flux and heat flux reduction on the external vane surface, for different cases. For the uniform inlet case, it is clear that, in the regions with sufficient internal cooling, local heat flux is always larger than other region, see in Figure 14(a). As mentioned above, the main function of film cooling is forming a protective layer to decrease the heat flux transfer from the mainstream to the vane structure. In Figure 14(a), it is clear that relatively lower local heat flux can be observed in the regions covered by film cooling, especially on the aft portion of the vane. Although the main function of film cooling is not directly cooling the vane surface, region with negative local heat flux can be observed on the both surface sides. On the suction side, regions with negative local heat flux can be observed in the regions close to the downstream of the film cooling holes and in the regions close to the trailing edge. On the pressure side, regions with negative local heat flux locate close to the upstream of the row D1 film cooling holes. As mentioned above, the strong acceleration of the mainstream rapidly decreases static temperature in the regions close to the stagnation line on the suction side and to the trailing edge on the pressure side. Thus, the introducing of film cooling can easily lead to negative local heat flux in those regions. For the hot streak only case, local heat flux increases significantly in the regions close to the film cooling holes of forward portion where under the direct impingement of the hot streak, see in Figure 14(b). Apart from the influence of temperature redistribution, swirl transports the film coolant from the leading edge toward the midspan which enhances the coverage of film cooling in those regions. In comparison, migrating film coolant worsens the film coolant coverage in the hub and tip end-wall

Preprints (www.preprints.org) | NOT PEER-REVIEWED | Posted: 21 April 2021 doi:10.20944/preprints202104.0568.v1

regions which increases the local heat flux in those regions. For hot streak and positive swirl case, regions with negative heat flux can be observed on the suction side because of the enhancement of the film cooling coverage, see in Figure 14(c). Figure 15 shows the distribution of local heat flux reduction on the external surface, for different cases. A positive value means a decrease in the local heat flux because of the coatings. Compare Figure 14 with Figure 15, it is clear that, the distribution of local heat flux reduction in analogy to that of local heat flux. In the regions with higher local heat flux, heat flux reduction is always larger than in other regions for the coated vane. In addition, negative value can be observed on the same regions with negative local heat flux, where adding coatings decrease the heat flux transfer from the vane to the mainstream.

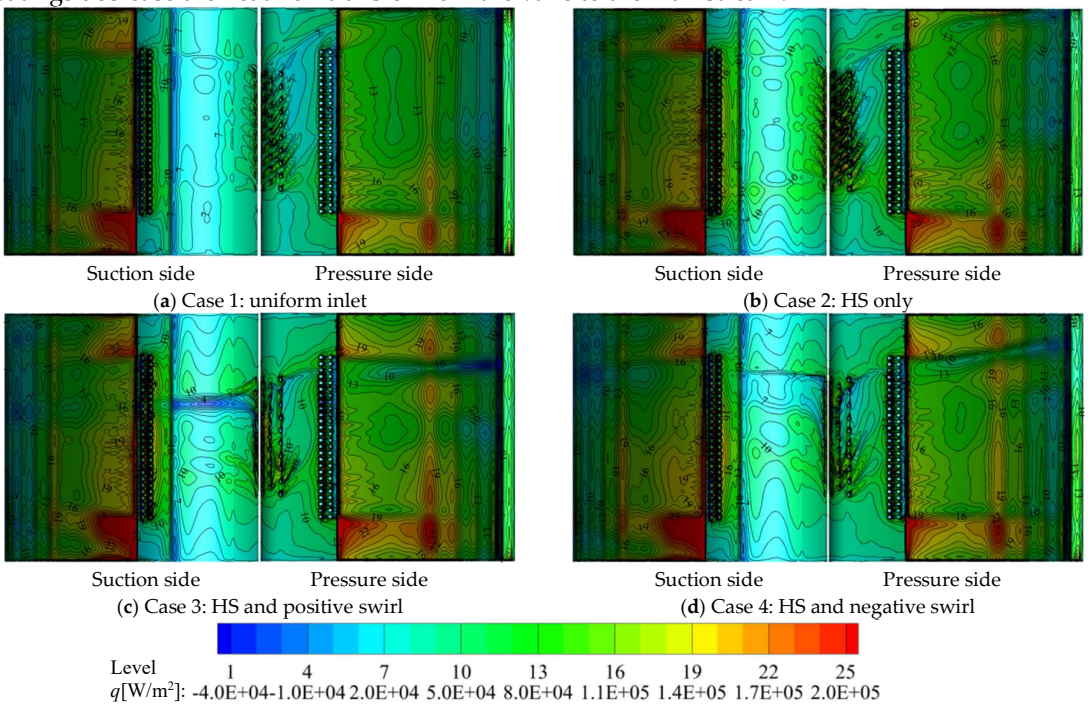

Figure 14. Local heat flux distribution for different cases.

Figure 16 shows the distribution of local heat flux and heat flux reduction along the external surface at cutting planes of the 25 % span, 50 % span and 75 % span, for different cases. In Figure 16, it is clear that sharp fluctuations of the local heat flux and heat flux reduction profile can be observed in the region close to the film cooling holes, for all the cases. Despite the film cooling holes regions, negative heat flux can be observed in the region between about 32 % C_{ax} and 34 % C_{ax}, as well as the region around 99.5 % C_{ax} on the suction side, for the uniform inlet case, see in Figure 16(b). On the pressure side, negative heat flux locates between about -93 % C_{ax} and -95 % C_{ax} of the midspan. Compare with uniform inlet case, the increment of heat flux and heat flux reduction on the suction side is higher than that of the pressure side, especially on the midspan, see in Figure 16(b). Compare with the uniform inlet case, the heat flux reduction increases from about -1200 W/m² to 1479 W/m² at the 25 % C_{ax} of the midspan on the suction side. On the pressure side, the heat flux reduction increases from about 21000 W/m² to 32113 W/m² on the -25 % C_{ax} of the midspan. On the pressure side of aft portion, the local heat flux and heat flux reduction of the Case 3 is higher than that of the Case 4 on the 25 % span. On the suction side of aft portion, higher heat flux and heat flux reduction can only be observed on the cutting plane of the 25 % span, for the Case 4. As mentioned above, the main function of TBCs is forming protective coatings layers with lower heat flux conductivity to decrease the heat flux transfer from the hot flow to the vane structure. However, in the region with negative local heat flux of coated vane, adding coatings decreases the heat flux transfer from the vane to the mainstream. Thus, their negative influences on the overall cooling performance should be clearly revealed for the coated vane.

Preprints (www.preprints.org) | NOT PEER-REVIEWED | Posted: 21 April 2021 doi:10.20944/preprints202104.0568.v1

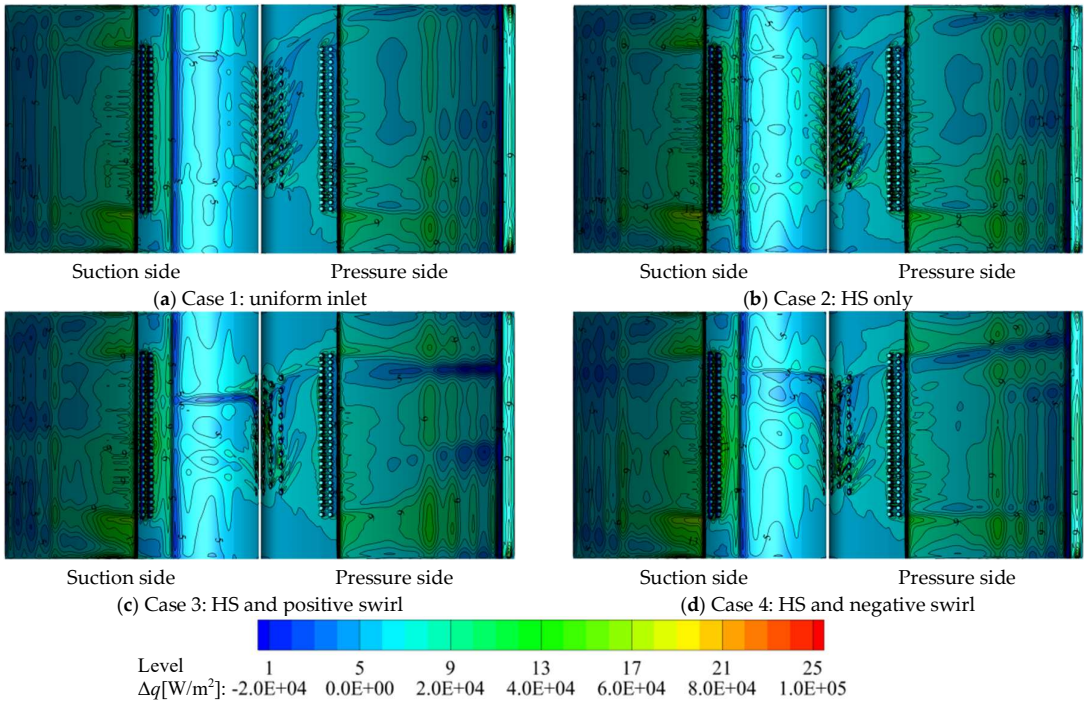

Figure 15. Local heat flux drop distribution for different cases.

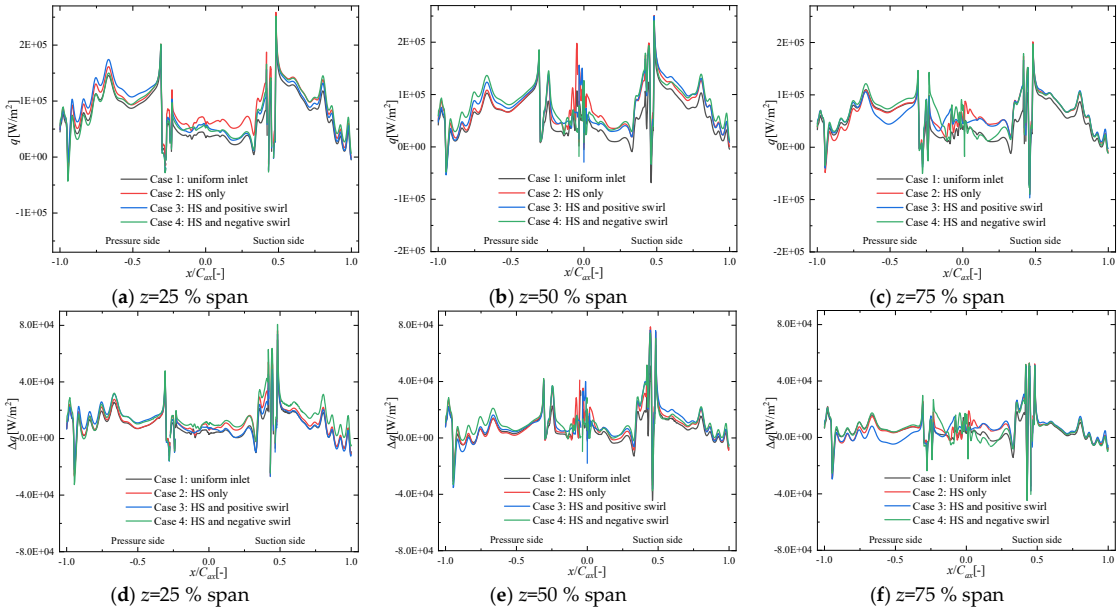

Figure 16. Local heat flux and heat flux drop distribution along the vane surface.

3.4. Influence of hot streak and swirl on the cooling performance of the coated vane

Figure 17 shows the overall cooling effectiveness distribution of the coated vane, for different cases. For coated vane, the overall cooling effectiveness distribution is just an analogy to that of the uncoated vane. Lower overall cooling effectiveness locates the region close to the stagnation line, especially in the region close to the end-wall the forward portion. On the aft portion of the vane, regions with higher cooling effectiveness locate in the region near radical cooling channels, while relatively lower cooling effectiveness can be observed between the adjacent cooling channels [23-24]. For the hot streak only case, cooling effectiveness decreases on the whole mental surface, especially on the suction side of the forward portion, see in Figure 17(b). Compare with the hot streak only

Preprints (www.preprints.org) | NOT PEER-REVIEWED | Posted: 21 April 2021 doi:10.20944/preprints202104.0568.v1

case, cooling effectiveness increases on the suction side of forward portion. While it decreases on the aft portion of the vane, especially in the tip region, for the Case 3 and Case 4, see in Figure 17(c) and Figure 17(d). Figure 18 shows the cooling effectiveness increment because of the coatings, for different cases. For the uniform inflow case, in the regions with sufficient internal cooling, the cooling effectiveness increment is always larger than other regions, especially in the region close to radical cooling channels, see in Figure 18(a). The cooling effectiveness increment decreases on the region covered by film cooling, especially in the region downstream of the film cooling holes and region close to the trailing edge with lower or negative local heat flux. Compare with the uniform inlet case, the cooling effectiveness increment increase on the whole mental surface, especially on the suction side of the forward portion, see in Figure 18(b). Under the influence of the swirl, radical migration of coolant improves the coverage of film cooling on the region close to the midspan. Besides, it decreases the cooling effectiveness increment on those regions, see in Figure 18(c) and Figure 18(d).

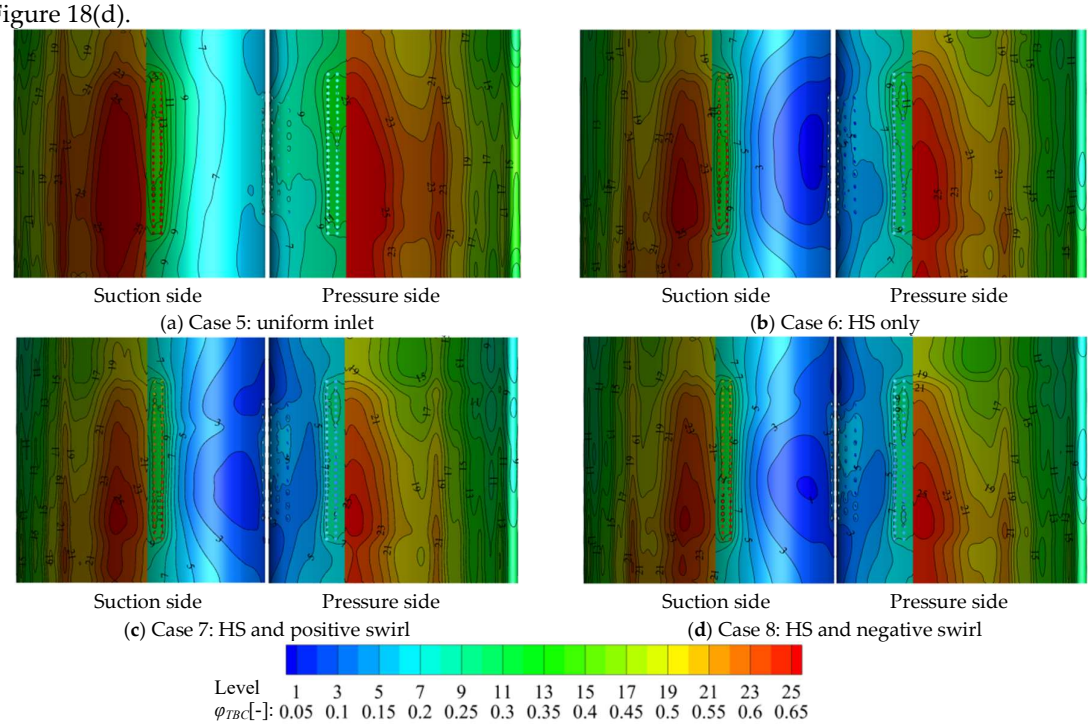

Figure 17. Overall cooling effectiveness distribution of coated vane for different cases.

Figure 19 shows the overall cooling effectiveness and cooling effectiveness increment distribution along the subtract surface at cutting planes of the 25 % span, 50 % span and 75 % span, for different cases. Compare Figure 4 with Figure 19, the overall cooling effectiveness of coated vane is larger than that of uncoated vane on the whole mental surface. In addition, the difference of overall cooling effectiveness between different coated cases is smaller than that of the uncoated vane. In Figure 19, it is clear that lower cooling effectiveness increment can be observed on the forward portion of the vane, where a local maximum can be observed close to the stagnation line, for all the cases. Cooling effectiveness increment decreases along vane surface to where the local minimum is reached on both surface sides. For the uniform inlet case, the local minimum can be observed on the -19 % C_{ax} where close to the downstream of the film cooling holes on the pressure side, see in Figure 19. Besides, the local minimum can be observed on the 31 % C_{ax} on the suction side where close to region with negative local heat flux, see in Figure16 and Figure19. Further along the vane surface, other local minimums can also be observed close to film cooling holes where with negative heat flux. It is noted that the substrate metal temperature of coated vane is influenced by the temperature of mainstream and coolant, temperature gradient of coatings and substrate, as well as the distance of the cooling channels from the surface. For the coated vane, the largest temperature gradient is located inside the coatings. In the regions with higher local heat load, the

Preprints (www.preprints.org) | NOT PEER-REVIEWED | Posted: 21 April 2021 doi:10.20944/preprints202104.0568.v1

temperature gradient of coatings is always larger than other regions. Thus, larger cooling effectiveness increments can be observed in those regions. Also, local heat load decrease in the region under the coverage of film cooling which decreases the temperature gradient inside the coatings and thus declines cooling effectiveness increment in those regions for the coated vane. In the region with negative local heat flux, adding coatings decreases the heat flux transfer from the vane structure to the mainstream which decreases the cooling performance in those regions. Consequently, the local minimum of cooling effectiveness increment because of the coatings can be observed in those regions.

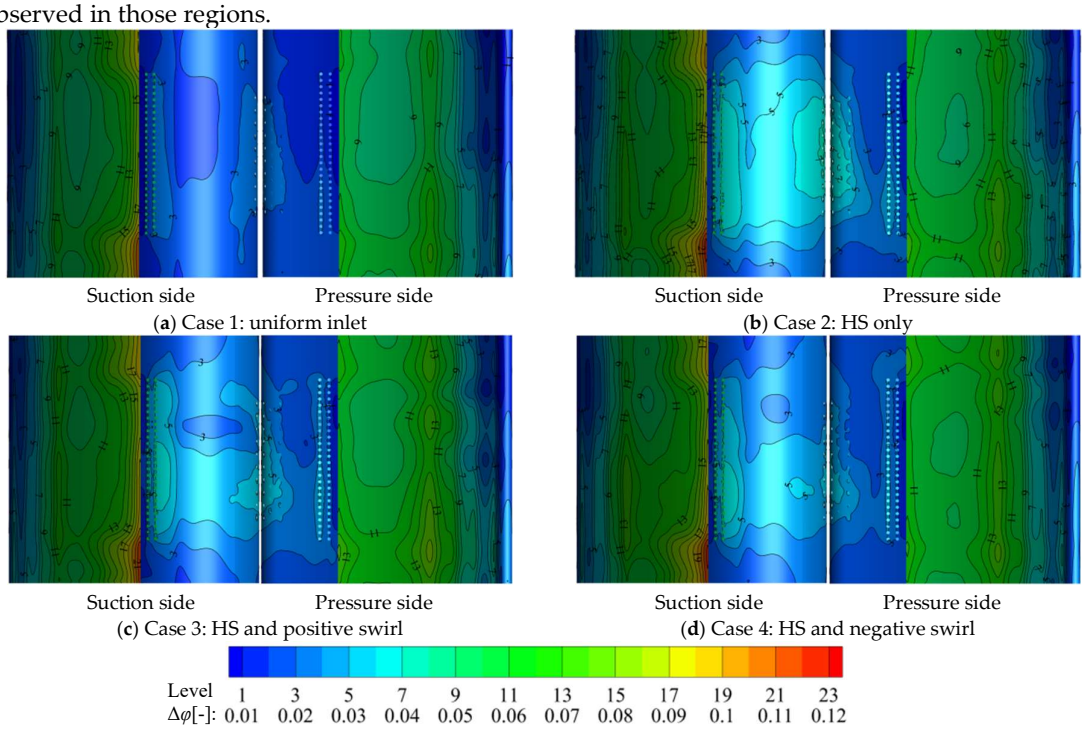

Figure 18. Cooling effectiveness increment distribution of coated vane for different cases.

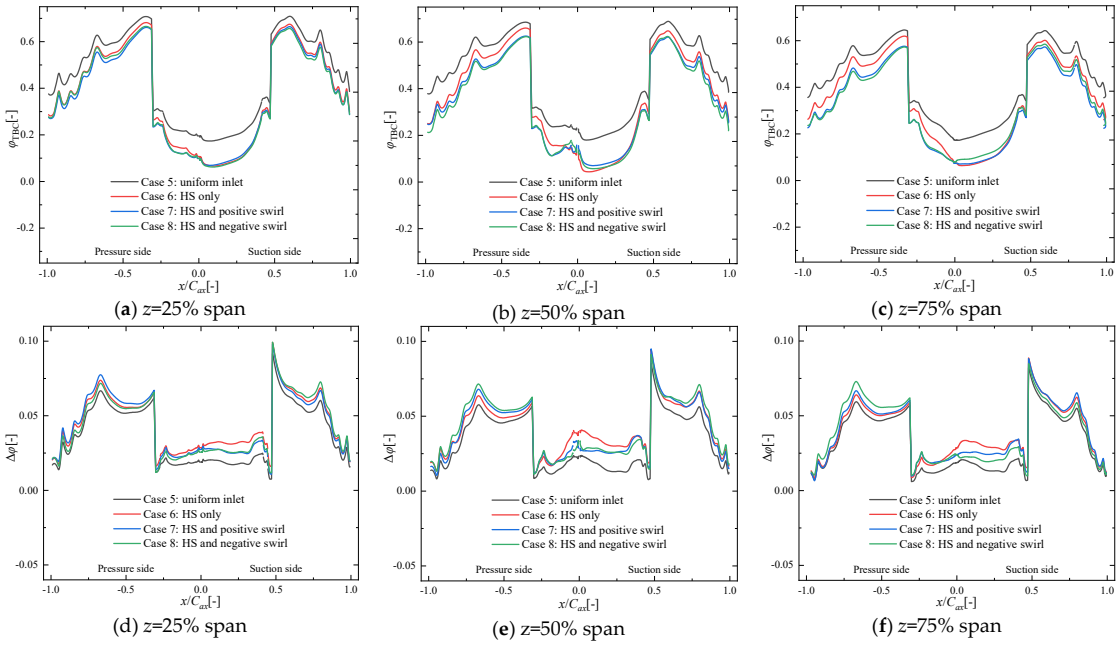

Figure 19. Cooling effectiveness and cooling effectiveness increment along the vane surface.

Compare with the uniform inlet case, the cooling effectiveness increment increases on the whole surface, especially on the suction side of the vane, see in Figure 19. Compare with the uniform inlet case, the cooling effectiveness increment increase from 0.015 to 0.021, at the -25 % C_{ax} of the midspan on the pressure side. In comparison, the cooling effectiveness increment increases from 0.013 to 0.03, at the 25 % C_{ax} of the midspan on the suction side. On the aft portion of the vane, the overall cooling effectiveness increment of the Case 3 is larger than the Case 4 on the pressure side of the 25 % span and on the suction side of the 75 % span. Compare with the Case 4, the overall cooling effectiveness increment change from about 0.058 to 0.064 at the -75 % C_{ax} of the 25 % span for the Case 3. In comparison, the overall cooling effectiveness increment change from 0.051 to 0.056 at the 75 % C_{ax} of the 75 % span for the Case 3.

4. Conclusions

This paper studies the combined influences of the hot streak and swirl on the cooling performances of the NASA C3X guide vane coated with or without TBCs. The following conclusions can be drawn:

(1) Even with uniform velocity inlet condition, hot streak core can be stretched as it impinged the leading edge which causes higher heat load on the suction side of forward portion. The interaction between hot streak and swirl significantly redistributes the hot streak core. On the passage inlet plane, positive swirl leads to a hotter tip region on the suction side. In the radial direction, a local maximum of 781.7 K locates near the 55% span. In comparison, negative swirl leads to a hotter hub region on the pressure side. In the radial direction, a local maximum of 782.1 K locates close to the 45% span.

(2) Under the influence of swirl, migration of coolant improve the coverage of film cooling close to the midspan, while close to the hub and tip region, the film cooling coverage decrease simultaneously. Positive swirl leads to a more negative impact on film cooling coverage on the tip region. In comparison, negative swirl leads to a more negative impact on the hub region. Considering the negative influence of inlet swirl flow, enhancing cooling arrangements design is necessary in the hub and tip region.

(3) In the regions with enough internal cooling, adding coatings leads to larger cooling effectiveness increment for the coated vane. In addition, local heat load decreases in the region under the coverage of film cooling which decreases the temperature gradient inside the coatings and thus declines cooling effectiveness increment in those regions for the coated vane. Thus, improving internal cooling is the guarantee of improving the cooling performance for the coated vane.

(4) Local minimum of cooling effectiveness increment can be observed in the regions with negative local heat flux for the coated vane, where adding coatings decreases the heat flux transfer from the substrate surface to the mainstream, and thus decreases the overall cooling performance in those regions for the coated vane. Thus, avoiding over-cooling in the regions downstream the film cooling holes and tailing edge of vane surface should be appropriately taken into consideration during the cooling arrangements design process for the coated vane.

Author Contributions: In this paper, Li Shi carried out the simulation, and wrote this paper. Hanze Huang and Yuanfeng Lu improved the discussions; Shunsheng Xu and Chen Ge improved this paper overall.

Funding: This research was funded by National Natural Science Foundation of China, grant number 51806184 and Natural Science Foundation of Hunan Province, grant number 2019JJ50590.

Conflicts of Interest: The authors declare no conflict of interest.

Nomenclature

x, y, z	cartesian coordinates [mm]
C_{ax}	axial chord [mm]
$C_{p,BC}$	specific heat capacity of bond coating [J/(kg·K)]

 doi:10.20944/preprints202104.0568.v1

$C_{p,f}$	specific heat capacity of fluid [J/(kg·K)]
$C_{p,SUB}$	specific heat capacity of substrate [J/(kg·K)]
$C_{p,TC}$	specific heat capacity of top coating [J/(kg·K)]
$C_{p,TGO}$	specific heat capacity of thermally grown oxide [J/(kg·K)]
p	Pressure [Pa]
p_{ref}	reference pressure [285.13×103Pa]
T	metal surface temperature without TBC [K]
T_c	inlet temperature of cooling air [K]
T_{ref}	reference temperature [701 K]
T_{TBC}	metal surface temperature with TBC [K]
T_w	vane local wall temperature [K]
T_∞	inlet temperature of mainstream [K]
T'	surface temperature outside the coating [K]
ΔT_{TBC}	relative reduction of the substrate temperature due to coating
ρ_{SUB}	density of substrate [kg/m3]
ρ_{TC}	density of top coating [kg/m3]
ρ_{TGO}	density of thermally grown oxide [kg/m3]
ρ_{BC}	density of bond coating [kg/m3]
φ_{TBC}	overall cooling effectiveness of the coated vane
$\Delta\varphi$	overall cooling effectiveness increment due to coating
ΔT_{comb}	the temperature rise across the combustion chamber
u_{ax}	inlet axial
u_{rad}	radial velocity
u_{tan}	Combustion chamber
Greek letters	
α	swirl angle
β	pitch angle
φ	overall cooling effectiveness of the uncoated vane
Abbreviations	
NGV	nozzle guide vane
TBC	thermal barrier coating
HS	hot streak
CHT	conjugate heat transfer
LE	leading edge
PS	pressure side
SS	suction side
PSW	positive swirl
NSW	negative swirl
Subscripts	

w	wall
c	cooling air
ref	reference
∞	mainstream

References

1. Je-Chin, H.; Michael, H. Recent studies in turbine blade internal cooling. Heat Transf. Res. 2010, 41(8), 803-828. [CrossRef]
2. Zhang, J. Z. ; Zhu, X. D. ; Huang, Y. ; Wang, C. H. Investigation on film cooling performance from a row of round-to-slot holes on flat plate. Int. J. Therm. Sci. 2017, 118, 207-225. [CrossRef]
3. Padture; N., P. Thermal barrier coatings for gas-turbine engine applications. Science. 2002, 296(5566), 280-284. [CrossRef]
4. Feuerstein, A. ; Knapp, J. ; Taylor, T. ; Ashary, A. ; Bolcavage, A. ; Hitchman, N. Technical and economical aspects of current thermal barrier coating systems for gas turbine engines by thermal spray and EBPVD: a review. J. Therm. Spray Technol. 2008, 17(2), 199-213. [[CrossRef]
5. Liu, J. H. ; Liu, Y. B. ; He, X. ; Liu, L. Study on TBCs insulation characteristics of a turbine blade under serving conditions. Case Stud in Therm Eng. 2016, 8, 250-259. [CrossRef]
6. Prasert, P. ; Soemsak, Y. ; Suwin, S. ; Daniele, D. ; Huazhao, X. ; Jianhua, W. Investigation of cooling performances of a non-film-cooled turbine vane coated with a thermal barrier coating using conjugate heat transfer. Energies, 2018, 11(4), 1000. [CrossRef]
7. Shi, L. ; Sun, Z Y. ; Lu, Y. F. , The Combined influences of film Cooling and thermal barrier coatings on the cooling performances of a Ffilm and internal cooled vane. Coatings. 2020, 10, 861. [CrossRef]
8. Li, Y. ; Su, X. ; Yuan, X. The effect of mismatching between combustor and HP vanes on the aerodynamics and heat load in a 1-1/2 stages turbine. Aerosp Sci Technol. 2019, 86, 78-92. [CrossRef]
9. Wang, Z. ; Wang, D. ; Wang, Z. ; Feng, Z. Heat transfer analyses of film-cooled HP turbine vane considering effects of swirl and hot streak. Appl. Therm. Eng. 2018, 142. [CrossRef]
10. Zhang, K. ; Li, Z. ; Li, J. Effect of swirl on the vane endwall aerothermal performance with endwall misalignment at transonic condition. Int. J. Heat Mass Transf. 2019, 144, 118662. [CrossRef]
11. Povey, T. ; Chana, K.S. ; Jones, T.V. ; Hurrion, J. The Effect of Hot-Streaks on HP vane surface and endwall heat transfer: an experimental and numerical study. J. Turbomach. 2007, 29. [CrossRef]
12. Povey, T. ; Qureshi, I. Developments in Hot-Streak simulators for turbine testing. J. Turbomach. 2009, 131, 83-97. [CrossRef]
13. Stewart, W.R. ; Bogard, D.G. Experimental thermal field measurements of film cooling above the suction surface of a turbine vane. J Eng Gas Turb Power. 2017, 137, 102604. [CrossRef]
14. Simone, S. ; Montomoli, F. ; Martelli, F. Analysis on the Effect of a Non-uniform Inlet Profile on Heat Transfer and Fluid Flow in Turbine Stages. J. Turbomach. 2012, 134, 011012. [CrossRef]
15. Feng, Z. ; Liu, Z. ; Shi, Y. ; Wang, Z. Effects of hot streak and airfoil clocking on heat transfer and aerodynamic characteristics in gas turbine. J. Turbomach. 2016, 138, 021002.021001-021002.021010. [CrossRef]
16. Qureshi, I. ; Povey,T. A combustor-representative swirl simulator for a transonic turbine research facility. Proceedings of the Institution of Mechanical Engineers Part G Journal of Aerospace Engineering. 2011, 225 , 737-748. [CrossRef]
17. Jacobi, S. ; Mazzoni, C.M. ; Chana, K. ; Rosic, B. Investigation of unsteady flow phenomena in first vane caused by combustor flow with swirl. J. Turbomach. 2016, 139, 041006. [CrossRef]
18. Jacobi, S. ; Rosic, B. Thermal investigation of integrated combustor vane concept under engine-realistic condition. J. Turbomach. 2017, 139, 021005. [CrossRef]
19. Quresh, I. ; Beretta, A. ; Chana, K. ; Povey, T. Effect of aggressive inlet swirl on heat transfer and aerodynamics in an unshrouded transonic HP turbine. J. Turbomach. 2012, 134, 61023-61021.[CrossRef]
20. Qureshi,I. ; Smith, A.D. ; Povey, T. HP vane aerodynamics and heat transfer in the presence of aggressive inlet swirl. J. Turbomach. 2013, 135, 021040. [CrossRef]
21. Werschnik, H. ; Hilgert, J. ; Wilhelm, M. ; Bruschewski, M. ; Schiffer, H.P. Influence of combustor swirl on endwall heat transfer and film cooling Effectiveness at the large scale turbine rig. J. Turbomach. 2017, 139, 081007. [CrossRef]

22. Schmid, G. ; Krichbaum, A. ; Werschnik, H. ; Schiffer, H.P. The impact of realistic inlet swirl in a 1-1/2 stage axial turbine. ASME, 2014. [CrossRef]
23. Hylton, L. D. ; Nirmalan, V. ; Sultanian, B. K. ; Kauffman, R. M. The effects of leading edge and downstream film cooling on turbine vane heat transfer; NASA Technical Report; NASA-CR-182133; NASA, Washington, DC, USA, 1988. [CrossRef]
24. Hylton, L. D. ; Mihelc, M. S. ; Turner, E. R. ; Nealy, D. A. ; York, R. E. Analytical and experimental evaluation of the heat transfer distribution over the surfaces of turbine vanes; NASA Technical Report; NASA-CR-168015; NASA Lewis Research Center, Cleveland, OH, USA, 1982. [CrossRef]
25. Ke, Z. ; Wang, J. Conjugate heat transfer simulations of pulsed film cooling on an entire turbine vane. Appl. Therm. Eng. 2016, 109, 600-609. [CrossRef]
26. C. Koupper, Unsteady multi-component simulations dedicated to the impact of the combustion chamber on the turbine of aeronautical gas turbines, Ph.D. thesis, Universite de Toulouse. 2015. [CrossRef]
27. Jiang, Y. ; Zheng, Q. ; D Ping, Yao, J. ; Hai, Z. ; Jie, G. Conjugate heat transfer analysis of leading edge and downstream mist–air film cooling on turbine vane. Int.J. Heat Mass Transf. 2015, 90, 613-626. [CrossRef]